



# Isotopic compositions ( $\delta D$ , $\delta^{18}O$ ) and end-member mixing for the control interface in a complex tidal region

Rongrong Xie<sup>a,b,c</sup>, Ling Zhen<sup>a,\*</sup>, Xianzhong Wu<sup>d</sup>, Jiabing Li<sup>a,b,c,\*</sup>

<sup>a</sup> College of Environmental and Resource Science, Fujian Normal University, Fuzhou 350007, China

<sup>b</sup> Key Laboratory of Pollution Control and Resource Recycling of Fujian Province, Fujian Normal University, Fuzhou 350007, China

<sup>c</sup> Digital Fujian Environmental Monitoring Internet of Things Laboratory, Fuzhou 350007, China

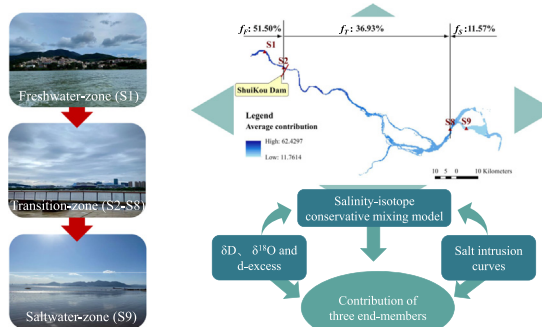
<sup>d</sup> Fuzhou Research Academy of Environmental Sciences, Fuzhou 350013, China

## HIGHLIGHTS

- The  $\delta D$  and  $\delta^{18}O$  depleted from August to November and then enriched next April.
- The isotopes of hydrogen and oxygen enriched significantly in the saltwater zone.
- The annual average  $f_F$ ,  $f_T$  and  $f_S$  were 51.50 %, 36.93 % and 11.57 %, respectively.
- Evaporation and moisture sources affected isotopes and end-member mixing.

## GRAPHICAL ABSTRACT

Contributions of freshwater, transition zone and saltwater end-members.



## ARTICLE INFO

Editor: Frederic Coulon

### Keywords:

Hydrogen and oxygen isotopes  
Conservative mixing model  
Salinity  
Tidal reach

## ABSTRACT

Identifying the mixing processes of waters and currents in tidal reach is an important aspect of environmental management to protect freshwater resources and prevent water pollution. In this study, three field investigations conducted in a typical tidal reach in August, November and the following April focused on two isotopes ( $\delta D$  and  $\delta^{18}O$ ) and salinity. A salinity-isotope conservative mixing model was established to differentiate water flows of the important control interface (CI) from freshwater, transition zone and saltwater end-members. Results suggested that the average  $\delta D$  and  $\delta^{18}O$  values during the ebb and flood tides depleted from August to November, then enriched significantly in the following April and were even higher than those in August. The  $\delta D$  and  $\delta^{18}O$  values in the saltwater zone enriched markedly compared with those in freshwater zone and transition zone due to the stronger evaporation occurring in the saltwater zone. Based on the revised model, the average contributions of freshwater end-member, transition zone end-member and saltwater end-member in three months were, respectively, 51.50 %, 36.93 % and 11.57 %. However, the contributions of freshwater and transition zones in April end-member were equivalent (47.45 % vs 44.31 %). Meanwhile the largest contribution of saltwater end-member was 20.56 % and occurred in August. The proportions of three end-members that contributed to CI changed with different evaporation scenarios and moisture sources of precipitation. Our research provides important information that furthers our understanding of the isotopes and their applications to environmental management in estuarine regions.

\* Corresponding authors at: 8 Shangsang Rd, Fuzhou 350007, China.  
E-mail addresses: [zhenling0@163.com](mailto:zhenling0@163.com) (L. Zhen), [lijabing@fjnu.edu.cn](mailto:lijabing@fjnu.edu.cn) (J. Li).

## 1. Introduction

Tidal reaches, which are the transition interval between land and sea, feature both an estuary and a river (Xie et al., 2017). Water circulation, nutrient transformation and aquatic ecosystems in the tidal reach are extremely complex due to the changeable freshwater-saltwater environment (Neubauer, 2013; Liu et al., 2017; Heiss et al., 2017). In these areas, the decline in freshwater input and increasing intrusion of high salinity water in tidal areas have become worldwide environmental problems due to the many river-built gates and dams at the basin scale (Neubauer, 2013; Gao et al., 2018; Ke et al., 2021). Water mass processes and saltwater intrusion have made a significant impact on the distribution of nutrients and other biogenic elements, and marine ecosystems, such as algal blooms and mariculture activities (May et al., 2010; Gong and Shen, 2011; Lao et al., 2022a, 2022b). How to trace the effect of freshwater and saltwater on the aquatic environment in the control interface (CI) is important so that we comprehend the pollution migration process; it has now garnered much scientific attention (Barlow and Reichard, 2010; Werner et al., 2013; Guo et al., 2017; Xu et al., 2018).

A good understanding of water mass processes in complex tidal reaches will deepen our knowledge of estuarine productivity and biogeochemical processes, as it is critical for management authorities to properly protect already limited freshwater resources and improve water quality in estuaries (Xu et al., 2018). Traditionally, the freshwater masses were usually characterized by dissolved oxygen, pH and hydrodynamic model, while seawater masses were distinguished by the relationship between the potential temperature and salinity along with density variations (Sengupta et al., 2013; Xu et al., 2020). However, the traditional tracers were less conservative and could not follow the water itself (Bigg and Rohling, 2000). Since stable isotope tracers have become an important tool for determining water, carbon, nitrogen and trace element fluxes and cycle in estuarine systems (Bauch et al., 1995; Fry, 2002; Liu et al., 2016), the isotopes of hydrogen ( $\delta D$ ) and oxygen ( $\delta^{18}O$ ) are regarded as excellent proxies of water bodies to identify the water cycle. They indicate the origin and formation of different water masses and water bodies, tracking the processes and pathways of the water cycle, estimating the rate at which the water cycle moves and determining the interconversion between different water bodies (Gat, 1996; Clark and Fritz, 1997; Gibson et al., 2002; Stalker et al., 2009; Jung et al., 2020), and thereby quantify the contribution of different water mass processes (Gibson et al., 2005; Gammons et al., 2006; Schiavo et al., 2009; Zannoni et al., 2019; Wu et al., 2021).

In addition, the coupling of salinity,  $\delta D$  and  $\delta^{18}O$  in estuarine areas has been successfully used to discriminate different water masses. This is because such indices exhibit similar behavior during the phase transitions between evaporation and freezing and mixing of water from different origins and salinity (Currell et al., 2015; Dubinina et al., 2017). The  $\delta D$  and  $\delta^{18}O$  typically changed across estuarine salinity gradients from freshwater to the sea (Lian et al., 2016; Dubinina et al., 2017). The evaporation in estuarine areas could lead to co-varying linear changes in salinity,  $\delta D$  and  $\delta^{18}O$  (Epstein and Mayeda, 1953). Meanwhile the slope and intercept of  $\delta^{18}O$ -salinity linear regression for coastal oceans could be more sensitive when freshwater dominates the mixing areas (Bigg and Rohling, 2000; Nuttle et al., 2000). Moreover, deuterium excess ( $d\text{-excess} = \delta D - 8 \cdot \delta^{18}O$ ) was a favorable complementary indicator for stable isotopes, because  $\delta D$  and  $\delta^{18}O$  are easily affected by equilibrium fractionation and kinetic fractionation as phases change in water bodies (Merlivat and Jouzel, 1979). The  $d\text{-excess}$  and  $\delta D/\delta^{18}O$  analysis could serve to indicate the climatic conditions for moisture producing and different levels of evaporation (Harvey and Welker, 2000; Celle-Jeanton et al., 2001). Usually, higher transpiration fractions may lead to relatively low  $d\text{-excess}$  (Xia et al., 2022).

The software known as IsoSource (IsoSource 1.3; EPA, USA) is based on multisource linear mixed model while Stable Isotope Analysis in R (SIAR) is based on the Bayesian isotope mixing model (Wu et al., 2021). These have been widely applied to identify the nitrate pollution source (Hu et al., 2018; Guo et al., 2020; Niu et al., 2021). Applying stable isotopes to models has

inherent possibilities and advantages. Peng et al. (2005) modified the Rayleigh fractionation model to understand the isotope response of precipitation by evaporation and transpiration. Gross et al. (2019) clearly defined the transport time of the water source with substantial fractional evaporation using the isotope-based water age model. However, all these mixing models were limited to solving the contributions of specific sources and limited by source data (Phillips, 2001).

In the tidal reach, the freshwater/saltwater changeable environment is evident and pollution accumulates easily due to the bidirectional flow and contributions of varieties of pollution sources which are also changeable. However, the source of contamination is not easily identified and collected in the tidal reach. Hence, the isotopic values of mixed estuarine samples rather than pollution source were focused. The conservative mixing of riverine and seawater end-members by using concentrations to weight the end-member riverine and oceanic isotopic compositions were raised (Spiker, 1980). Then the concept of conservative mixing of stable isotopes across estuarine salinity emerged since freshwater-seawater mixing creates an isotope imprint (Fry, 2002). However, previous research has focused mainly on the coastal areas and the effect of freshwater masses here was usually underrated compared with the seawater masses (Reyes-Macaya et al., 2022; Zhou et al., 2022). Poorly studied isotopes and models in tidal reach do represent a huge gap in our knowledge.

In this paper, the  $\delta D$  and  $\delta^{18}O$  over a period of three months were monitored in tidal reach and a salinity-isotope conservative mixing model was devised to comprehend the mixing process of freshwater and saltwater in the tidal reach. The findings documented here will prove to be important for saving the environment and managing economic and social development in tidal reaches.

## 2. Material and methods

### 2.1. Research area

The Minjiang River is the longest river (2959 km) in Fujian Province, China, and it has the seventh highest annual runoff in the country, covering a watershed of 60,922 km<sup>2</sup> (Hu et al., 2014). In this paper, the tidal reach from Shuikou Dam to the Minjiang estuary, with an approximate length of 117 km, was selected as the study area (25°55' ~ 26°18'N, 118°48' ~ 119°22'E, Fig. 1). The upstream discharge is dominated by the Shuikou Dam and the minimum discharge is 308 m<sup>3</sup>·s<sup>-1</sup> (Xie et al., 2017). The Minjiang estuary has a typical semi-diurnal tidal regime with diurnal inequality, and the tidal cycle lasts nearly 12.4 h. The average tidal range is 4.5 m but the maximum tidal range can exceed 6 m (Xie et al., 2017). The Jingangtui cross-section was set as the freshwater/saltwater control interface (CI) by the Fuzhou government. Due to the effect of the local sub-tropical monsoon climate, there is abundant precipitation and the annual rainfall varies from 1100 to 1600 mm (Zhang et al., 2016). The annual average temperature is 19.9 °C and it generally ranges from 9.8 to 32.3 °C.

### 2.2. Field investigations and data collection

Three field surveys for isotopic compositions ( $\delta D$ ,  $\delta^{18}O$ ) were conducted on 19th August 2020, 16th November 2020 and 24th April 2021 and the respective tidal ranges during the sample collections were 4.56 m, 5.93 m and 4.53 m in Minjiang estuary. A total of 9 monitoring stations were installed to investigate the freshwater/saltwater contributions to the CI (Fig. 1). The 9 monitoring stations were divided into three zones according to salinity and tidal effects. Stations S1 and S2 are located in the upstream of the Shuikou Dam and represent the freshwater zone contribution. The transition zone extended from Shuikou Dam to the CI (Station S8) and it served to calculate the transition zone's contribution, where the manure and sewage inputs were the main pollution sources especially in the North Channel (Zhang et al., 2015). Meanwhile, the effect of the downstream of the CI was regarded as the saltwater zone contribution. The detailed sampling times during the ebb tide and the flood tide were designed for the lowest and highest water level of each station, respectively

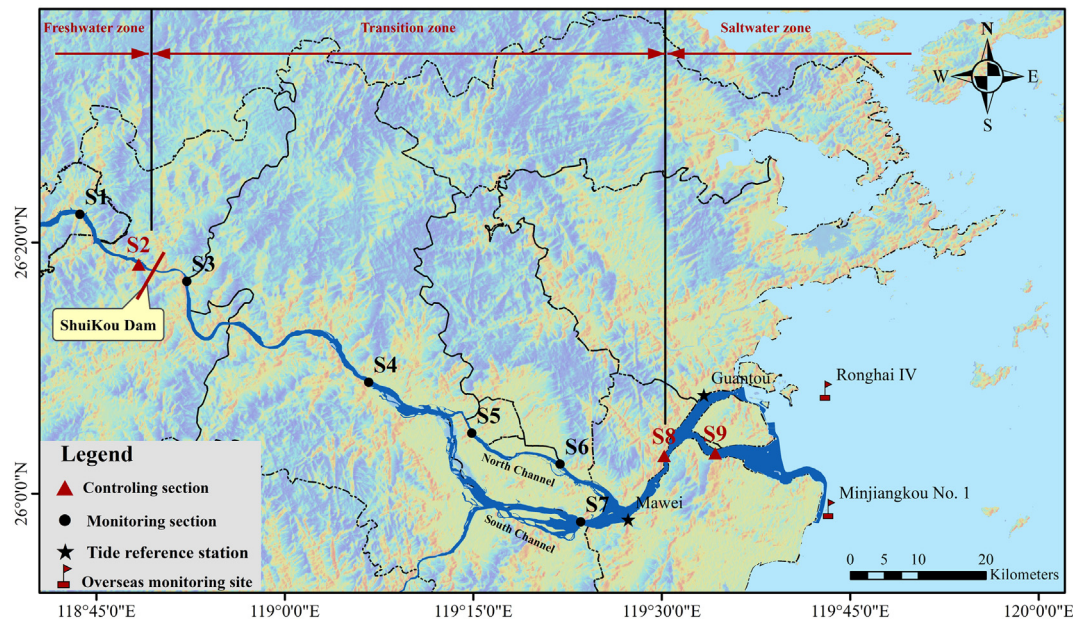


Fig. 1. Sampling sites and small watershed in the study location.

(Table 1). The samples were not taken simultaneously at the same time in this study due to different tidal cycle times between high tide and low tide of each station, which were calculated according to the tidal variations of the Mawei and Guantou reference stations on each sampling day (Supplementary Fig. S1) and the distances between sampling stations. However, all the samples of each station could indicate the full effects of freshwater in the upstream or saltwater in the downstream.

Given the influential reach of the reciprocating flow, the water samples were collected from station S1 to S9 during the ebb tide and from S4 to S9 during the flood tide, respectively. All the water samples were collected

from 0.5 m below the water surface in the midstream and the detailed sampling information is listed in Supplementary Table S1. Meanwhile the salinity was monitored in the field using a salinometer (CT-3081, Kedida, China) and the accuracy of the salinity measurements was within 0.02. According to the UNESCO (1985) definition, the practical salinity scale is a conductivity ratio and thus has no units. For the  $\delta D$  and  $\delta^{18}O$  isotope testing, the water samples were filtered through a 0.22  $\mu m$  filter and stored at  $-4^{\circ}C$  for testing. The  $\delta D$  and  $\delta^{18}O$  were measured at Environmental Stable Isotope Lab, Chinese Academy of Agricultural Science (CAAS). For  $\delta D$ , a total of 1uL water sample was injected into a furnace tube packed

**Table 1**  
Salinity,  $\delta D$ ,  $\delta^{18}O$  and d-excess for samples (Mean  $\pm$  SD).  $\bar{\alpha}$  represents the average of values, and units is ‰.

Month	Sampling time		Ebb tide				Flood tide				
			Salinity	δD	δ <sup>18</sup> O	d-excess	Sampling time	Salinity	δD	δ <sup>18</sup> O	d-Excess
19th August 2020	S1	10:40	0.09	−38.4 ± 0.02	−6.0 ± 0.26	9.73 ± 2.090					
	S2	10:06	0.03	−38.7 ± 0.09	−6.2 ± 0.12	10.50 ± 1.016					
	S3	9:19	0.03	−40.4 ± 0.20	−6.2 ± 0.17	9.16 ± 1.531					
	S4	8:45	0.02	−39.7 ± 0.17	−6.1 ± 0.08	9.40 ± 0.497	13:51	0.05	−41.0 ± 2.36	−6.2 ± 0.19	8.85 ± 3.847
	S5	7:57	0.04	−40.0 ± 0.28	−6.8 ± 0.10	14.36 ± 1.099	13:09	0.02	−40.2 ± 0.07	−6.8 ± 0.02	14.32 ± 0.219
	S6	7:09	0.04	−40.2 ± 0.17	−6.5 ± 0.27	11.83 ± 2.338	12:20	0.53	−40.5 ± 0.53	−6.7 ± 0.07	12.74 ± 0.006
	S7	7:05	0.53	−42.2 ± 1.19	−6.4 ± 0.12	8.60 ± 0.248	12:14	2.56	−38.8 ± 0.03	−6.1 ± 0.01	10.03 ± 0.113
	S8	6:13	3.30	−37.4 ± 1.56	−6.6 ± 0.36	15.28 ± 1.351	11:14	11.0	−29.1 ± 2.47	−4.8 ± 0.11	9.61 ± 1.604
	S9	5:43	11.9	−19.3 ± 0.91	−3.1 ± 0.20	5.44 ± 0.703	10:45	18.9	−28.3 ± 0.17	−4.6 ± 0.03	8.13 ± 0.391
	$\bar{\alpha}$		1.77	−37.4 ± 6.91	−6.0 ± 1.11	10.48 ± 3.006		5.51	−36.3 ± 5.97	−5.9 ± 0.95	10.61 ± 2.403
16th November 2020	S1	10:52	0.03	−41.8 ± 0.06	−6.8 ± 0.01	12.77 ± 0.050					
	S2	10:20	0.04	−42.3 ± 0.36	−6.9 ± 0.01	13.01 ± 0.484					
	S3	9:52	0.03	−42.5 ± 0.55	−6.9 ± 0.11	13.04 ± 0.318					
	S4	8:55	0.04	−41.5 ± 0.33	−6.5 ± 0.08	10.54 ± 0.998	14:36	0.02	−43.1 ± 1.91	−6.7 ± 0.24	10.59 ± 0.012
	S5	8:11	0.04	−41.6 ± 1.06	−6.5 ± 0.07	10.08 ± 0.520	13:41	0.04	−41.6 ± 0.01	−6.3 ± 0.09	9.10 ± 0.759
	S6	7:26	0.07	−41.3 ± 0.04	−6.7 ± 0.03	12.24 ± 0.232	12:48	0.24	−41.6 ± 0.66	−6.6 ± 0.23	10.94 ± 2.490
	S7	7:22	0.46	−41.6 ± 1.66	−6.6 ± 0.11	11.49 ± 0.807	12:42	1.69	−39.6 ± 1.89	−6.4 ± 0.33	11.37 ± 0.750
	S8	6:34	2.38	−38.9 ± 0.10	−6.5 ± 0.03	13.27 ± 0.139	11:41	6.40	−33.7 ± 0.10	−5.6 ± 0.00	11.28 ± 0.102
	S9	6:06	11.2	−26.3 ± 2.90	−4.1 ± 0.46	6.69 ± 0.792	11:07	14.4	−24.3 ± 0.35	−3.7 ± 0.04	5.11 ± 0.686
	$\bar{\alpha}$		1.59	−39.8 ± 5.13	−6.4 ± 0.87	11.46 ± 2.120		3.80	−37.3 ± 7.17	−5.9 ± 1.14	9.73 ± 2.409
24th April 2021	S1	10:40	0.02	−38.0 ± 2.44	−6.0 ± 0.14	10.06 ± 1.331					
	S2	10:02	0.02	−37.3 ± 1.04	−5.9 ± 0.04	9.68 ± 0.690					
	S3	9:38	0.02	−37.4 ± 0.72	−6.0 ± 0.03	10.36 ± 0.981					
	S4	8:47	0.02	−37.3 ± 2.29	−5.9 ± 0.11	9.76 ± 1.410	13:48	0.02	−42.6 ± 4.69	−6.6 ± 0.54	10.23 ± 0.383
	S5	7:47	0.02	−35.1 ± 0.73	−5.8 ± 0.05	11.55 ± 1.130	13:12	0.02	−36.3 ± 2.88	−6.0 ± 0.21	11.59 ± 1.164
	S6	6:52	0.03	−35.8 ± 2.93	−5.9 ± 0.30	11.74 ± 0.504	12:25	0.08	−41.2 ± 2.67	−6.2 ± 0.39	8.45 ± 0.420
	S7	6:48	0.18	−36.5 ± 2.64	−6.4 ± 0.21	14.48 ± 0.919	11:45	1.30	−32.3 ± 4.53	−5.8 ± 0.36	14.33 ± 1.635
	S8	6:08	2.25	−28.7 ± 3.62	−5.5 ± 0.04	15.37 ± 3.969	11:07	8.76	−25.1 ± 1.85	−4.5 ± 0.24	11.12 ± 0.061
	S9	5:30	9.30	−23.6 ± 1.86	−4.2 ± 0.09	10.05 ± 1.102	10:37	14.1	−18.5 ± 3.36	−3.4 ± 0.70	8.35 ± 2.229
	$\bar{\alpha}$		1.32	−34.4 ± 4.93	−5.7 ± 0.61	11.45 ± 2.114		4.05	−32.7 ± 9.40	−5.4 ± 1.23	10.68 ± 2.233



with 200–300 μm mesh chromium, which was put in the 1050 °C hot-zone of the furnace. As the carrier helium transported the sample through the furnace tube, the H<sub>2</sub>O was pyrolyzed to form H<sub>2</sub>. Then the product H<sub>2</sub> was analyzed by the Isotopic Liquid Water Analyzer L1115-I (Picarro, Santa Clara, California, USA). Referring to the δ<sup>18</sup>O, 1 μL of water sample was injected into a standard quartz furnace tube that contained 80 mm of low cost “black carbon” (Elementar part no. 03679910), which was located in the 1170 °C hot zone of the furnace. With a large amount of carbon available in the furnace, the H<sub>2</sub>O was pyrolyzed to form CO. This CO sample was then separated from any residual N<sub>2</sub> using a GC column held isothermally at 70 °C. The CO was then isotopically analyzed by the Picarro L1115-I. The accuracies of δD and δ<sup>18</sup>O were within 0.5 ‰ and 0.2 ‰, respectively.

The meteorological data of Fuzhou city including temperature, humidity and rainfall were collected from the Huiju website (<http://hz.hjhj-e.com>), which provides hourly meteorological data of many cities in China. The upstream discharge information was provided by the Fuzhou Environmental Science Research Institute, and the tidal range data were collected from the tidal website (<http://www.chaoxibiao.net>).

### 2.3. Expression of isotope data

The stable isotope ratios are expressed in delta (δ) units and a per mil deviation (‰) relative to the respective international standards:

$$\delta = \left( \frac{R_{\text{sample}}}{R_{\text{standard}}} - 1 \right) \times 1000 \quad (1)$$

where,  $R_{\text{sample}}$  represents the measured isotopic ratios of <sup>18</sup>O/<sup>16</sup>O, or <sup>2</sup>H/<sup>1</sup>H.  $R_{\text{standard}}$  denotes the Vienna Standard Mean Ocean Water (VSMOW) for H and O isotope analysis.

Deuterium excess (d-excess) is a useful parameter that provides additional information on the isotopic water cycle (Celle-Jeanton et al., 2001). It is calculated using the following formula (Dansgaard, 1964):

$$d - \text{excess} = \delta D - 8 \times \delta^{18}O \quad (2)$$

D-excess values, influenced by the monsoon climate, humidity and evaporation, varied regionally. Normally the d-excess value in the surface water is relatively lower, which indicates the evaporation and a supplement added to the water vapor source area (Clark and Fritz, 1997; Grassa et al., 2006).

### 2.4. Salinity-isotope conservative mixing model

In this paper, freshwater, transition zone and saltwater were defined as 3 end-members for the control interface according to the ranges of the bidirectional flow and salinity intrusion (Zhang et al., 2013; Liu et al., 2016; Xie et al., 2020). To evaluate contributions of freshwater/saltwater to the CI, a salinity-isotope conservative mixing model for these 3 end-members was established based on the 2 end-members mixing model raised by Fry (2002). This model builds on the well-established concepts of conservative mixing (Liss, 1976; Loder and Reichard, 1981). The freshwater carried a stable isotope signature distinct from that in seawater, while the freshwater-seawater mixing created an imprinted isotope. The discharges from different end-members were taken into account to assess the mixing of water mass compared with the traditional models. Considering the need for large amounts of isotope data and great uncertainty in the Bayesian isotope mixing model (Parnell et al., 2010; Xue et al., 2012; Niu et al., 2021), the model devised in this paper could determine the contributions of different inflows or nutrient loadings using fewer isotope data of rivers. As well, it is not subject to the incomplete statistics and limited sampled survey of pollution sources. The revised formulas are:

$$f_F + f_T + f_S = 1 \quad (3)$$

$$\delta_{\text{CI\_flood}} = \frac{f_F \cdot \text{Salinity}_{F\_ebb} \cdot \delta_{F\_ebb} + f_T \cdot \text{Salinity}_{T\_cal} \cdot \delta_{T\_ebb} + f_S \cdot \text{Salinity}_{S\_cal} \cdot \delta_{S\_flood}}{\text{Salinity}_{\text{CI\_flood}}} \quad (4)$$

where,  $f$  is the contribution of the end-member, and the subscripts F, T and S indicate the freshwater, transition zone and saltwater end-members, respectively.  $\delta_{\text{CI\_flood}}$  and  $\text{Salinity}_{\text{CI\_flood}}$  stand for the observed isotope and salinity of the CI in the flood tide, respectively.  $\delta_{F\_ebb}$  and  $\text{Salinity}_{F\_ebb}$  denote the observed isotope and salinity of the freshwater end-member in the ebb tide, respectively.  $\delta_{T\_ebb}$  is the observed isotope value of the transition zone end-member in the ebb tide,  $\delta_{S\_flood}$  is calculated value combined with the observed isotope value of the saltwater end-member and the research isotope value of the East Sea, China (Liu et al., 2016). The isotope value was homogenized because of the stronger evaporation effect in the flood tide.  $\text{Salinity}_{T\_cal}$  represents the calculated salinity of the transition zone because the salinity in this area could change between ebb tide and spring tide.  $\text{Salinity}_S$  is the observed value of the section in East Sea, China (Supplementary Fig. S2). Hence, the calculated salinity in this paper was revised by the observed salinity and the mixing water volumes based on the mass conservation:

$$\text{Salinity}_{T\_cal} = \frac{\overline{\text{Salinity}}_9 \cdot Q_S - \text{Salinity}_{F\_ebb} \cdot Q_F}{Q_T} \quad (5)$$

$$Q_S = Q_{\text{flood}} - Q' \quad (6)$$

$$Q_{\text{flood}} = \frac{(\text{High Water Mark} - \text{Low Water Mark}) \cdot \text{Area}_{\text{channel}}}{\text{Time}_{\text{tidal}}} \quad (7)$$

$$Q' = \frac{\text{Salinity}_S - \overline{\text{Salinity}}_9}{\text{Salinity}_S - \text{Salinity}_{F\_ebb}} \cdot Q_{\text{flood}} \quad (8)$$

where,  $\overline{\text{Salinity}}_9$  is the average salinity of saltwater end-member in the ebb and flood tide.  $Q_F$  is the average daily freshwater discharge of the Shuikou Dam in the experimental period,  $Q_T$  is the estimated discharge from the transition zone, and  $Q_S$  denotes the calculated tidal prism in the Minjiang tidal reach.  $Q_{\text{flood}}$  is the tidal discharge in tidal reach while  $Q'$  is the instant discharge when the spring discharge is equal to the ebb discharge.

Regarding the uncertainty analysis for the model, the sum of estimated proportional contributions of three end-members in the model is equal to 1. Considering the variability in the isotope composition in end-members, each estimated contribution of end-members should be a probability distribution within a given certain range. Hence, an uncertainty index ( $UI_{90}$ ), represents the uncertainty strength under a large probability scenario (90 %), and is used in this research. The term  $UI_{90}$  refers to the difference in the proportional contribution between the maximum and minimum values in the fast increase segment of 90 % cumulative probability divided by 90 (Ji et al., 2017). Here, the lower and upper values for 95 % confidence intervals of each end-member in the model were calculated by the formulas for confidence intervals (Phillips and Gregg, 2001). Following this each estimated contribution by the end-members should be a probability distribution with 95 % confidence intervals.

## 3. Results

### 3.1. Spatiotemporal distribution of salinity and stable isotopes

#### 3.1.1. Temporal variations during ebb and flood tides

Salinity in the ebb tide and flood tide followed the sequence: August > November > April (Table 1). In August 2020, the salinity ranged from 0.02 to 11.9 during the ebb tide and 0.02 to 18.9 during the flood tide. The salinity in November 2020 was 0.03–11.2 during the ebb tide and 0.02–14.4 during the flood tide. Then in April 2021, 0.02–9.3 during the ebb tide and 0.02–14.1 during the flood tide were determined. Fig. 2 shows the intrusion curves during ebb and floods over three months, where the origin of the longitudinal axis is located at S9 with the same salinity setting as S', L is the distance between S1 and S9, and 0.068 and 0.765 represent the

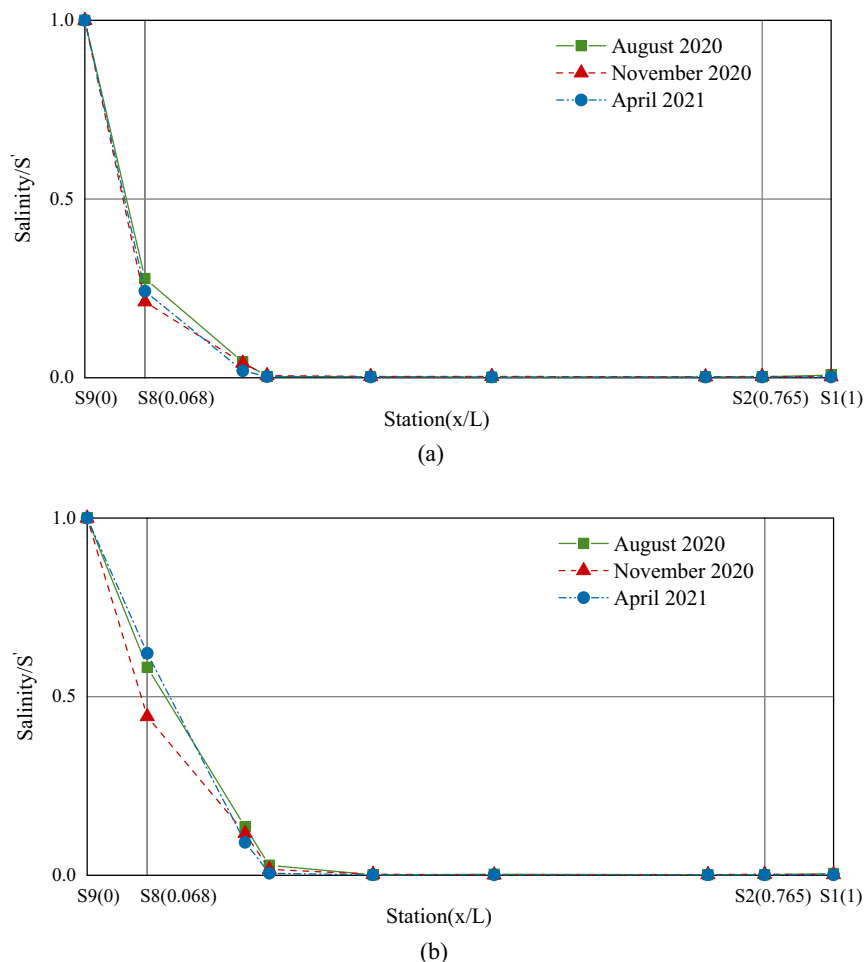


Fig. 2. Salt intrusion curves in Minjiang. In the figure, (a) represents the ebb tide and (b) represents the spring tide. The origin of the longitudinal axis is located at S9 with the same salinity setting as  $S'$ ,  $L$  is the distance between S1 and S9, while 0.068 and 0.765 represent the locations of S8 and S2, respectively.

locations of S8 and S2, respectively. The intrusion curve with a logarithmic convex shape indicated that the intrusion type for the Minjiang tidal reach had a recession shape, which occurs in narrow estuaries with a near-prismatic shape and a high river discharge.

The average  $\delta D$  and  $\delta^{18}O$  values during the ebb and flood tides in the study location depleted from August to November, and then enriched significantly the following April and were even higher than those in August (Table 1). The average  $\delta D$  in August, November and next April were  $-37.4$  ‰,  $-39.8$  ‰ and  $-34.4$  ‰ during the ebb tide and  $-36.3$  ‰,  $-37.3$  ‰ and  $-32.7$  ‰ during the flood tide, respectively. Meanwhile the average  $\delta^{18}O$  were  $-6.0$  ‰,  $-6.4$  ‰ and  $-5.7$  ‰ during the ebb tide and  $-5.9$  ‰,  $-5.9$  ‰ and  $-5.4$  ‰ during the flood tide. The  $\delta D$  and  $\delta^{18}O$  for the three months are plotted in Fig. 3 to compare with the local meteoric water line (LMWL) of Fuzhou based on the isotope data of Fuzhou precipitation station in 1985–1992 from International Atomic Energy Agency (Zhang et al., 2013) and the global meteoric water line (GMWL) (Craig, 1961). The slopes of the Minjiang River line declined from August to November, and then increased significantly the following April and even higher compared to August.

It could be seen that the Minjiang River line in April was  $\delta D = 7.638\delta^{18}O + 8.87$ , which was closer to the slope of LMWL and GMWL. Meanwhile in August and November, the slope of the river line deviated more compared with the LMWL. It has been observed in some research that the river lines had lower slopes, which suggested that all samples were affected by evaporation (Paulsson and Widerlund, 2020). The average d-excess values during ebb tides in the study region increased from 10.48 ‰ in August to 11.46 ‰ in November first, and subsequently

remained stable up to the following April (i.e., 11.45 ‰). During the flood tides, the average d-excess in August, November and next April were 10.61 ‰, 9.73 ‰, 10.68 ‰, respectively.

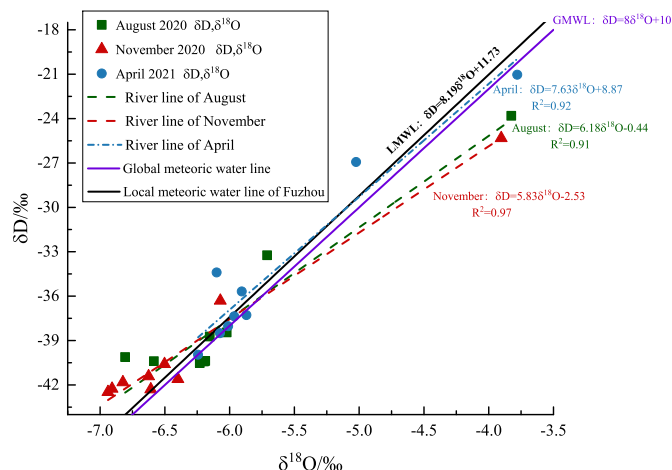


Fig. 3.  $\delta D$  and  $\delta^{18}O$  composition of Minjiang tidal reach in August 2020 (green square), November 2020 (red triangle) and April 2021 (blue circle). Also depicted are the meteoric water line in three months. The bold black line represents the local meteoric water line in Fuzhou (LMWL). The bold purple line represents the global meteoric water line (GMWL).

From the tidal scale, the  $\delta D$  in flood tide was lower than that in ebb tide at S4-S6 in three months, while the  $\delta D$  from S7 to S9 in flood tide was higher compared with ebb tide except S9 station in August. Referring to  $\delta^{18}O$ , there was the same trend between flood tide and ebb tide as the  $\delta D$  except that in November the  $\delta^{18}O$  at S5 and S6 during the flood tide was higher than those in ebb tide, which will be discussed later. The d-excess in flood tide was lower than that in the ebb tide at S4, S5 and S8, but higher at S6, S7 and S9 in August. From November to the following April, the d-excess at S4 station in flood tide was higher compared with that in the ebb tide. From S5 to S9 the overall d-excess values in the flood tide were lower except S5 for the next April.

The  $\delta D$  and  $\delta^{18}O$  values were positively correlated with salinity both in the ebb tide and the flood tide in the three months (Fig. 4a-b), especially in November and next April ( $P < 0.001$ ). Meanwhile in August, the slopes of  $\delta D$  and  $\delta^{18}O$  versus salinity diminished significantly in the flood tide compared with the ebb tide. In the latter, the slopes of  $\delta D$  and salinity from August to next April were 1.70, 1.39 and 1.48, respectively, and the intercepts were  $-40.41$  ‰,  $-41.96$  ‰ and  $-36.37$  ‰, respectively. Concerning the flood tide, the linear relationships were defined by slopes of 0.74, 1.24 and 1.48, respectively, and intercepts of  $-40.38$  ‰,  $-42.04$  ‰ and  $-38.66$  ‰, respectively. The linear relationships between  $\delta^{18}O$  and salinity in the ebb tide were defined by slopes of 0.26, 0.23 and 0.19, and intercepts of  $-6.44$  ‰,  $-6.77$  ‰ and  $-5.99$  ‰, respectively.

With reference to the flood tide, the slopes were 0.12, 0.2 and 0.2, and the intercepts were  $-6.51$  ‰,  $-6.63$  ‰ and  $-6.24$  ‰, respectively. There was no relationship between d-excess and isotopes both in ebb tide and flood tide (Supplementary Fig. S3), which confirmed two things: firstly, the upstream reach is mainly affected by continental mixing; and secondly, estuarine reach is mainly affected by kinetic fractionation (Masson-Delmotte et al., 2008; Kumar et al., 2018).

### 3.1.2. Spatial variations during ebb and flood tides

The spatial distribution of salinity in the three on-site surveys indicated that the salt intrusion head could reach S7 station (Table 1). The salinity increased distinctly at S7-S9 stations between ebb and flood tides. S7 revealed a freshwater changing to a slightly saline water environment, while S8 and S9 suffered from varying degrees of saline water. In the upstream from S1 to S6, salinity remained in the freshwater environment although the dual directional flow was observed at S4-S6, which indicated that the occurrence of salt intrusion required counterbalancing conditions (Xie et al., 2017). Salinity changes in the study area revealed that S8 was an important freshwater/saltwater CI.

The  $\delta D$  and  $\delta^{18}O$  values in freshwater zone and transition zone (S1-S7) retained virtually the same level expect for a small fluctuation. However, in the salt zone of S8 and S9, the isotopic values enriched significantly. The  $\delta D$  in ebb tide enriched from  $-42.2$  ‰,  $-41.6$  ‰ and  $-36.5$  ‰ to  $-19.3$  ‰,

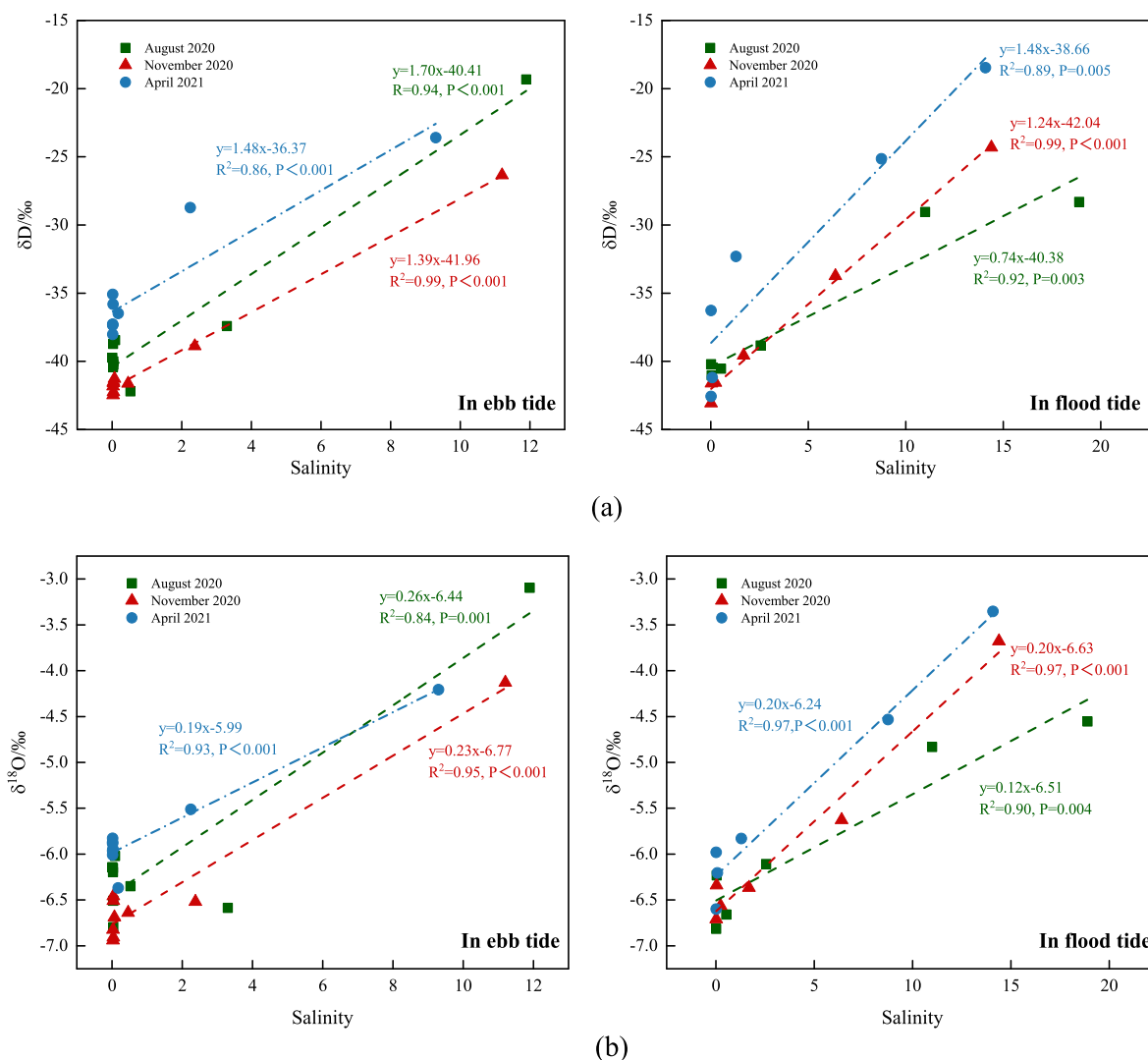


Fig. 4. The isotopes versus salinity and d-excess of Minjiang tidal reach in August 2020 (green square), November 2020 (red triangle) and April 2021 (blue circle). (a) represents  $\delta D$  versus salinity, (b) represents  $\delta^{18}O$  versus salinity.

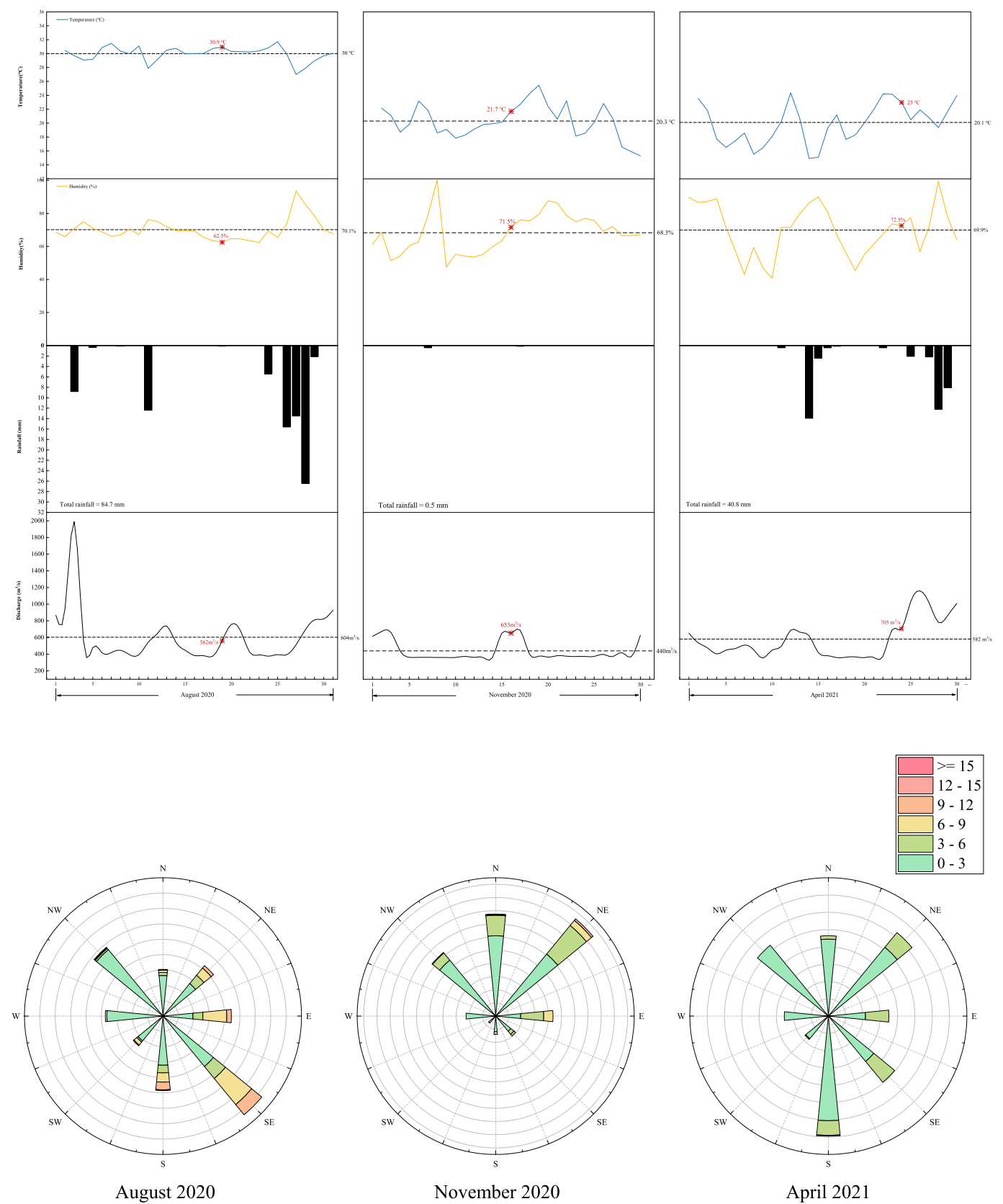


Fig. 5. Hydrometeorological conditions during the sampling months. The dash line represents the monthly average value of each parameter. The red stars represent the sampling day.

–26.3 ‰ and –23.6 ‰ in August, November and next April, respectively. In the flood tide the values enriched from –38.8 ‰, –39.6 ‰ and –32.3 ‰ to –28.3 ‰, –24.3 ‰ and –18.5 ‰, respectively. Similarly, the  $\delta^{18}\text{O}$  in ebb tide enriched from –6.4 ‰, –6.6 ‰ and –6.4 ‰ to –3.1 ‰, –4.1 ‰ and –4.2 ‰ in August, November and next April, respectively. Again for the flood tide the values enriched from –6.1 ‰, –6.4 ‰ and –5.8 ‰ to –4.6 ‰, –3.7 ‰ and –3.4 ‰, respectively. For the d-excess, the values in freshwater zone remained relatively stable and increased first from August to November and then declined to the August level in the following April. Meanwhile in the transition zone, the d-excess fluctuated in the range of 8.6–14.36 ‰ and 8.45–14.48 ‰ in August and next April, respectively. However, the variations of d-excess range in November were smaller (i.e., 9.10–12.24 ‰). In the saltwater zone, the d-excess dropped significantly

from S8 to S9. Especially in the ebb tide, the values waned from 15.28 ‰, 13.27 ‰ and 15.37 ‰ to 5.44 ‰, 6.69 ‰ and 10.05 ‰ in August, November and next April, respectively.

### 3.2. Variations in the hydrometeorological characteristics

The hydrometeorological characteristics on the sampling day in the research areas varied with the months (Fig. 5). Average temperatures on the sampling day in August, November and next April were 30.9 °C, 21.7 °C and 23.0 °C, respectively. In the meantime, the average humidity on the sampling day of three months amounted to 62.5 %, 71.5 % and 72.5 %, respectively. For the 2 weeks before the sampling day, the total rainfall varied from 12.8 mm in August to 0.4 mm in November and then

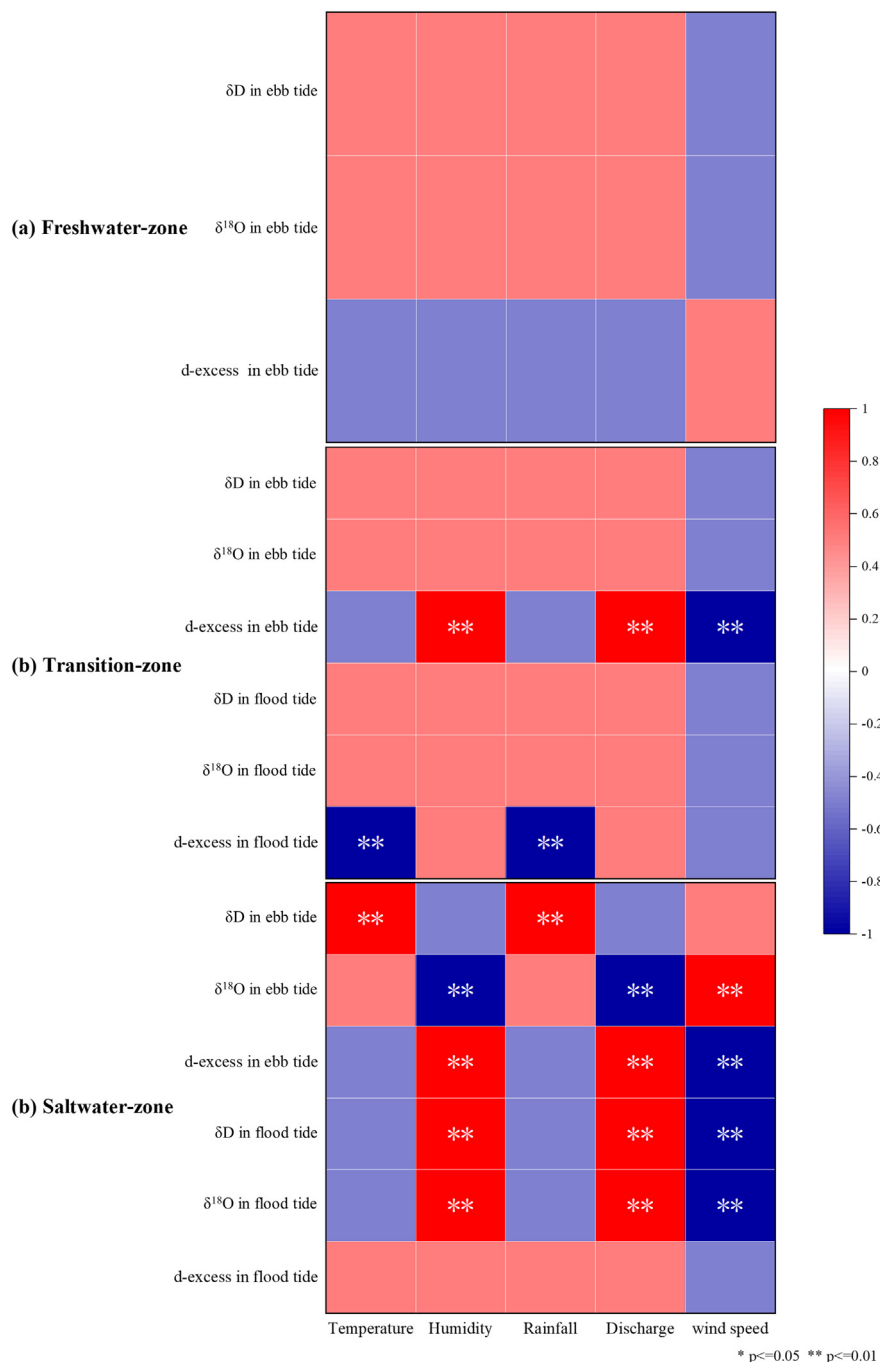


Fig. 6. Heat map of meteorological (temperature, relative humidity, rainfall, discharge and wind speed) with isotopes values ( $\delta\text{D}$ ,  $\delta^{18}\text{O}$ ) and d-excess. The correlation was calculated utilizing Spearman analysis.



to 17.1 mm in next April. The upstream discharges were 562 m<sup>3</sup>/s, 653 m<sup>3</sup>/s and 705 m<sup>3</sup>/s in August, November and next April, respectively, which were controlled by the Shuikou Dam operations. The hourly wind speeds in the same period were 3.2 m/s, 2.6 m/s and 2.0 m/s, respectively.

The Spearman analysis for isotope index ( $\delta D$ ,  $\delta^{18}O$  and d-excess) and the hydrometeorological characteristics are depicted in Fig. 6. In the freshwater zone, there was no clear correlation between isotope index and the hydrometeorological indices. Regarding the transition zone, d-excess in the ebb tide closely correlated with humidity, upstream discharge and wind speed. In the flood tide, d-excess significantly negatively correlated with temperature and rainfall, while in the saltwater zone, the  $\delta D$  in the ebb tide was significantly positively related with temperature and rainfall. The  $\delta D$  in the flood tide was very much linked to humidity, upstream discharge and wind speed. There was an important relationship between the  $\delta^{18}O$  and humidity, upstream discharge and wind speed both in ebb tide and flood tide scenarios. For d-excess, a significant relationship with humidity, upstream discharge and wind speed was found only in ebb tide.

### 3.3. Uncertainty analysis for mixing model

The cumulative probability distribution was explored to illustrate the uncertainty inherent in the contributions of three end-members (Fig. 7). The proportional contribution of  $f_S$  was stable because the  $UI_{90}$  was smallest (0.34). In 90 % probability, the proportional contribution of  $f_S$  occurred between 0.83 % and 31.48 %. However, the largest  $UI_{90}$  value (0.56) was observed for  $f_F$ , which meant that the proportional contribution of freshwater end-member exhibited the strongest uncertainty. Furthermore the contribution in 90 % probability ranged from 20.07 % to 70.14 % while the  $UI_{90}$  for  $f_T$  was 0.42. There are two reasons for the uncertainties inherent in quantifying the three end-members contribution to the CI. First is the isotope composition and source of three end-members, while the second is the isotope fractionation caused by the evaporation and hydrometeorological changes. In fact, the spatiotemporal distributions of isotopes in three end-members for the CI contribution are inevitable.

Although we consider that the salinity and discharge are constant within a short period of time, the intensity of salinity intrusion and regulated upstream discharge will cause variations in three end-members, which means that the contribution of  $f_F$  is highly uncertain. Considering the variations in the hydrometeorological characteristics, the isotope composition of three end-members changes considerably across space and time. Particularly, the proportion of  $f_S$  that contributed to CI varies with different evaporation scenarios and moisture sources of precipitation. The  $UI_{90}$

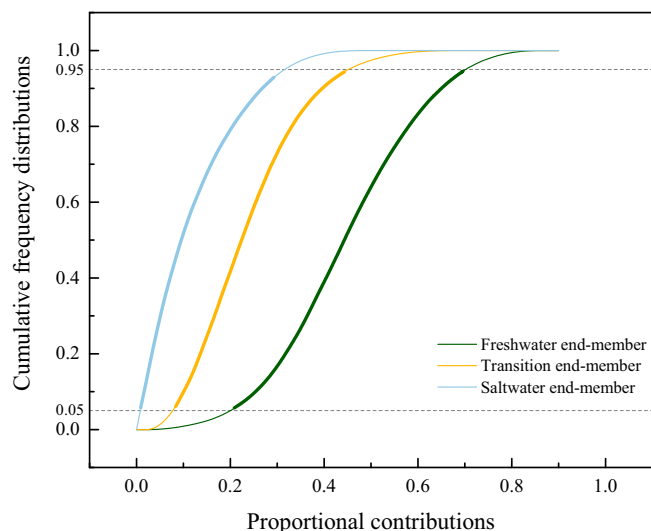


Fig. 7. Cumulative frequency distribution of the proportional contributions from three end-members based on the salinity-isotope conservative mixing model results.

values of three end-members were not low, which confirmed that fractionation was more important in influencing the uncertainty of the model.

### 3.4. End-member mixing for the control interface

In this paper, there were marked differences in rainfall and upstream discharges for the three months. The salinity-isotope conservative mixing model, the relevant parameters for the selected discharge and calculated salinity are defined in Supplementary Table S2 based on the collected data in three field surveys. The selected discharge and calculated salinity for transition zone and saltwater zone are calculated in Table 2. As well, based on the observed  $\delta D$  and  $\delta^{18}O$  values, the contribution ratios of three end-members were determined (Fig. 8). The contributions of freshwater end-member, transition zone end-member and saltwater end-member ( $f_F$ ,  $f_T$  and  $f_S$ ) in August were 46.61 %, 32.83 % and 20.56 %, respectively. Meanwhile the  $f_F$ ,  $f_T$  and  $f_S$  were 60.43 %, 33.66 % and 5.91 % in November and 47.45 %, 44.31 % and 8.24 % in next April, respectively. The freshwater end-member contributed the most in November with the lowest the rainfall and upstream discharge. It is noted that the highest  $f_S$  occurred in August, which was the same as the salinity intrusion which lasted longer during this month. For the area being investigated, the average contributions of three end-members were 51.50 %, 36.93 % and 11.57 %, respectively. The results had a probability of 90 %.

## 4. Discussion

### 4.1. Factors affecting isotopes

LMWL, which is mainly shaped by local meteorological conditions like seasonality of precipitation, the origin of the water vapor and secondary evaporation during rainy events, plays an important role in regional hydrogeological processes (Tian et al., 2001; Wu et al., 2014; Wu et al., 2015). The slope of Minjiang river line in August was obviously lower than that of LMWL, which was related to the intrusion of highest salinity waters in this month due to low runoff (Wu et al., 2021; Lao et al., 2022a). Besides, the backward trajectories originated and transported air masses precipitation in August all from oceanic moisture sources (Fig. 9A), which was quite different from local meteorological conditions. However, the lowest slope of the river line and the lowest isotope compositions in November were determined. During this month, there was virtually no precipitation and the discharge regulated by the Shuikou Dam was relatively stable compared with the value in other months (Fig. 5). This indicated that the rare precipitation and stable discharge could keep the isotopic composition at low levels by reducing the turbulence so that the evaporation rate decreased (Méès et al., 2020). Besides, the regulation of the Shuikou Dam changed the water velocity and discharge in different months. And the increasing residence time and enhancing mixing of reservoir water derived from upstream would result in the homogenization of reservoir water. The d-excess and  $\delta^{18}O$  values in November were more homogeneous because of the longer residence time and more completed mixing of the Shuikou reservoir, and thus small fluctuations of isotopes occurred in the downstream during ebb tide in this month. This situation was similar to other large rivers in China such as Yangtze River (Deng et al., 2016; Wu et al., 2022). In addition, the moisture source of the

Table 2

Selected discharge and calculated salinity profile for the transition zone and saltwater zone in the three sampled months.

Contribution zone	Selected discharge (m <sup>3</sup> /s)			Calculated salinity		
	August 2020	November 2020	April 2021	August 2020	November 2020	April 2021
Transition zone	4273	5418	2756	17.42	14.34	14.69
Saltwater zone	4835	6071	3461	30.79	26.24	27.25

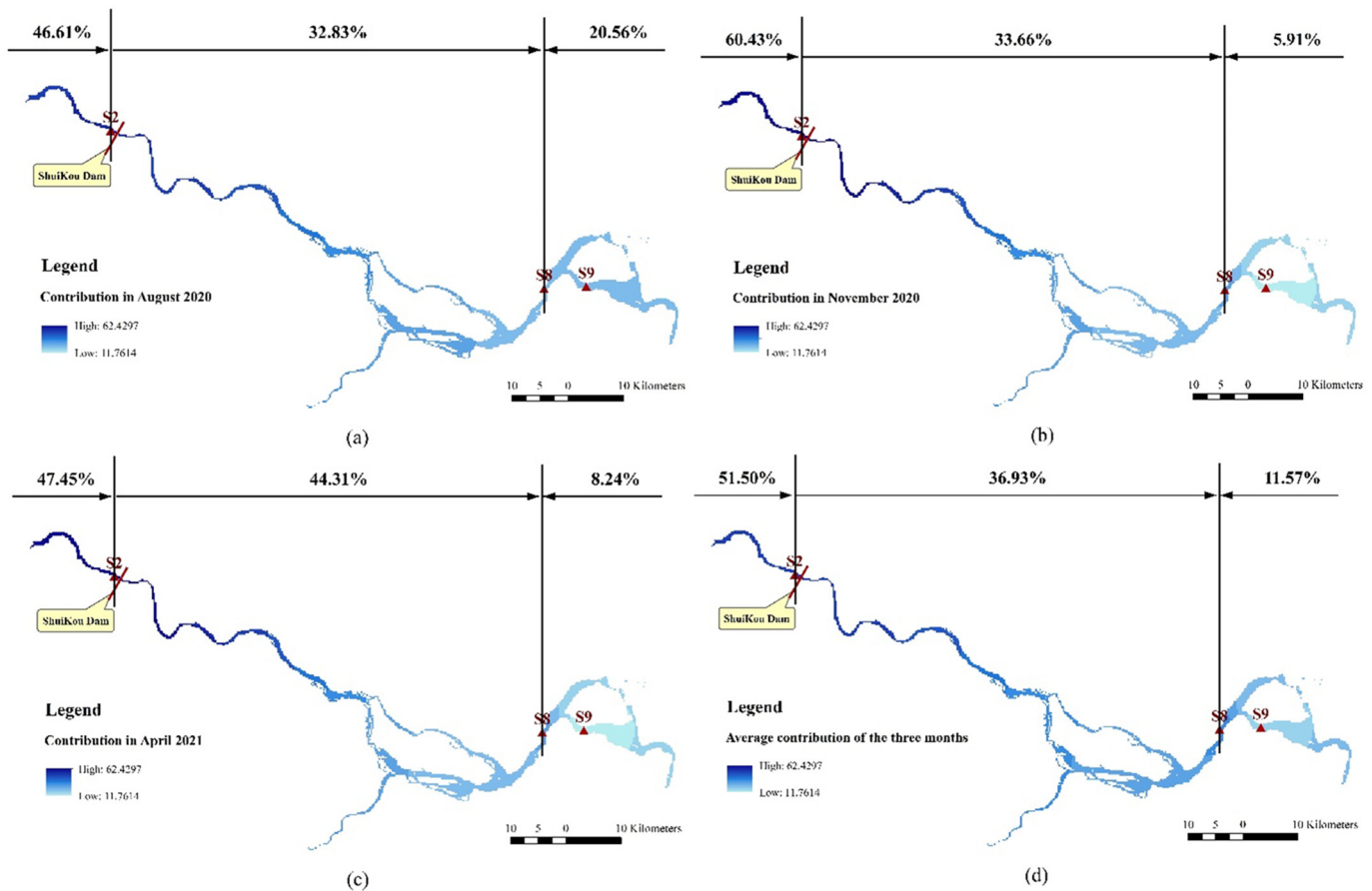


Fig. 8. Diagram of the model calculation results for the three months and average contribution of these months. In the figure, (a) represents August 2020, (b) represents November 2020, (c) represents April 2021, (d) represents the weighted-average contribution in the three months, respectively.

research area was composited by the inland (55.56 %) and oceanic (44.44 %) sources (Fig. 9B). The humidity was higher and the evaporation declined which led to the lower isotopic composition (Tian et al., 2008; Benetti et al., 2014; Xia et al., 2022). However, the river line in April was closer to the LMWL, which indicated the source from local precipitation (Price et al., 2012; Paulsson and Widerlund, 2020). Added to this, the local coastal source began to exhibit the percentage contribution of 21.81 % for the air mass in the research area (Fig. 9C). The air masses from the local areas for precipitation would have higher  $\delta D$  and  $\delta^{18}O$  (Bershaw et al., 2012). The month of April usually marked the early wet season and the  $\delta D$  and  $\delta^{18}O$  would be significantly enriched in precipitation after experiencing fractionation and enrichment throughout the whole dry season (Hu et al., 2019). That explained why the  $\delta D$  and  $\delta^{18}O$  in April enriched significantly and were higher than those in other months.

At the same time, the below-cloud secondary evaporation was rare because of the higher temperature and humidity (Xiong et al., 2021), which might possibly keep the d-excess of the precipitation at a higher level. Hence, the d-excess in the ebb tide was close to the value in flood tide at S5 station in April. However, the  $\delta D$  and  $\delta^{18}O$  values in August were lower than those in April especially in the downstream even under higher precipitation conditions, a situation caused by the weakened enrichment. This was due to the effect of the isotope fractionation under multiple rainfall processes of the same water mass (Matsuo and Friedman, 1967; Li et al., 2016). Furthermore, the moisture of precipitation in August all had an oceanic origin, which indicated the isotope values of the rainfall in this month were lower (Huang et al., 2018). The  $\delta D$  and  $\delta^{18}O$  in the saltwater zone (S8 and S9) enriched significantly in all three months and this supports the conclusion that  $\delta D$  and  $\delta^{18}O$  values in freshwater were usually less than those in seawater (Dansgaard, 1964). The end result was that the

isotope values during the flood tide were higher than during the ebb tide in the downstream tidal reach. However, the anomalous  $\delta^{18}O$  values in November in the middle reach (S5 and S6) during the flood tide were higher than that in the ebb tide, meaning that salinity intrusion could dominate the  $\delta^{18}O$  in longer reach under rare rainfall conditions.

The similar slope and intercept of  $\delta^{18}O$  and salinity during flood tide between November and next April could mean a similar isotopic composition existed (Kumar et al., 2018). The evidence for this is the closer temperature, humidity, wind speed and moisture source of precipitation in these two months. The average values of  $\delta D$ ,  $\delta^{18}O$  and d-excess in August are similar between the ebb tide and flood tide, especially since the difference in d-excess was only 0.13 ‰. This was usually caused by the higher rainfall consisting of a marine moisture source (Kopeck et al., 2018). As well, the non-normal change happening at S9 station may be due to the coupled effect from high rainfall and strong evapotranspiration, leading to significantly higher isotope values and lower d-excess values in the estuarine area (Araguás-Araguás and Froehlich, 1998; Singh et al., 2014).

The maximum isotope value that a water body can attain is governed by a combination of relative humidity and the atmosphere's isotopic composition. It is noted that the isotopic composition of the atmospheric water vapor is often assumed to be in equilibrium with local rainfall (Price et al., 2012). Besides,  $\delta D$ ,  $\delta^{18}O$  and d-excess are easily affected by meteorological conditions, i.e. temperature, relative humidity, precipitation and wind speed (Simmons et al., 2010; Puscas, 2019; Bryan et al., 2019). In the research area, the  $\delta D$  and  $\delta^{18}O$  of the saltwater zone were affected more strongly by meteorological conditions than other zones because the saltwater zone experiences a lot of evaporation, resulting in  $\delta D$  and  $\delta^{18}O$  being more easily changed by fractionation. The impact of climatic factors on isotopes is one of the challenges in earth surface isotope geochemistry

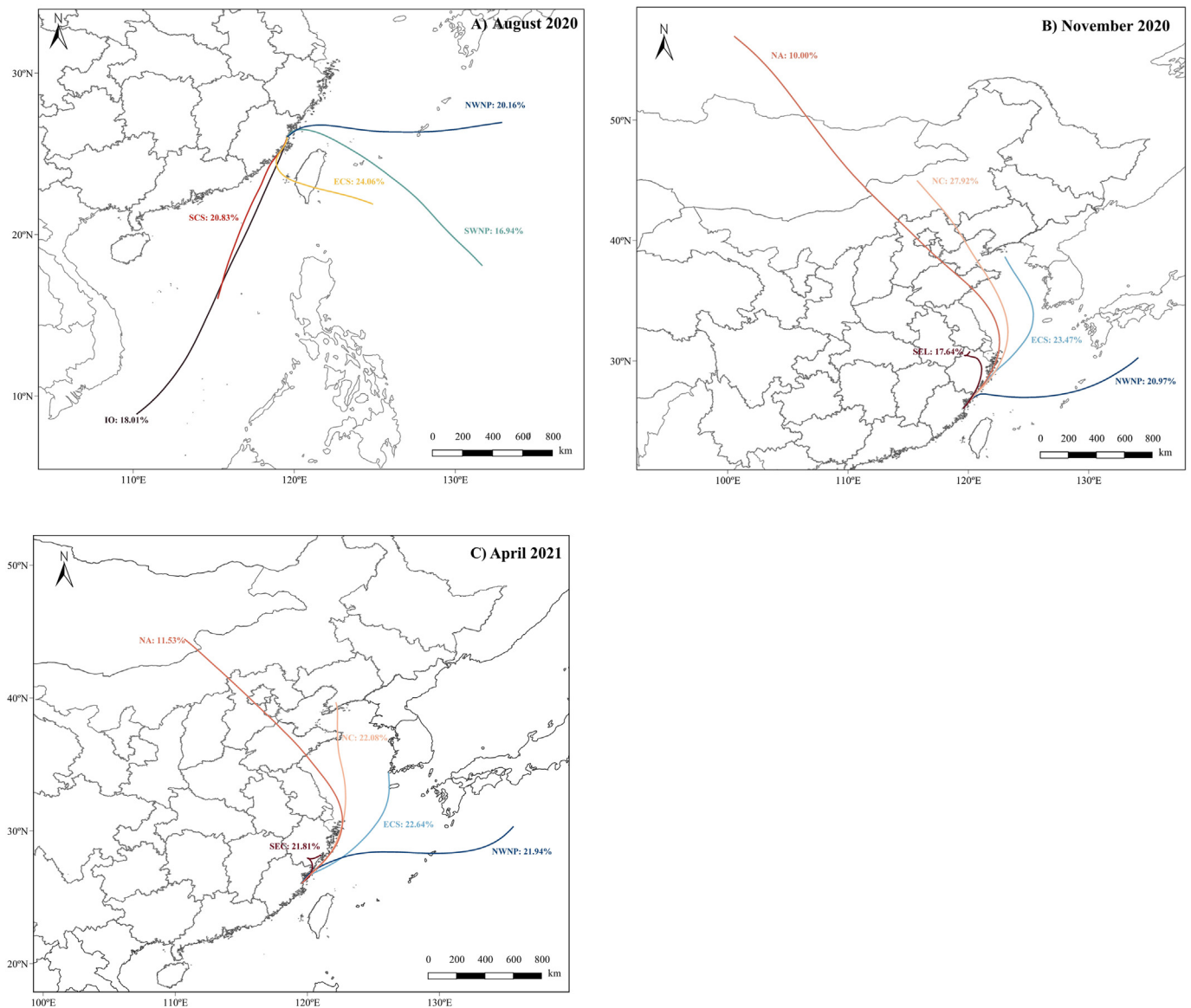


**Fig. 9.** Air mass backward trajectories from August 2020 to April 2021. The moisture source was found by [Chen et al. \(2021\)](#). In August 2020, all the moisture sources from the ocean, and the contribution of China Sea more than remote marine (WNWP represents the northern part of western North Pacific, SWNP represents the southern part of western North Pacific, ECS represents the East China Sea, SCS represents the South China Sea, and IO represents the Indian Ocean). In November 2020, more than half of the moisture source was terrestrial, and the greatest influence came from northern China (NC represents North China, NA represents North Asia and SEL represents Southeast Land of China). In April 2021, it is similar to November 2020, but the moisture source of NA is not as far away as November's, and the Southeast Coastal of China (SEC) replaced the SEL.

([Natali et al., 2021](#); [Oza et al., 2022](#)). Hence, in the revised model we used the homogenized isotope values of the observed isotope value and the research isotope value of the East Sea, China for the saltwater end-member in the flood tide. Besides, the  $\delta D$  in ebb tide was positively correlated with rainfall in the saltwater zone, which indicated that the secondary evaporation under cloud might occur during rain events. This is because precipitation is greater in heavy isotopes due to the secondary evaporation ([Peng et al., 2005](#)). However, the  $\delta^{18}O$  was mainly affected by humidity, discharge and wind speed, which is more sensitive than  $\delta D$  since  $\delta^{18}O$  will be more enriched than  $\delta D$  during evapotranspiration ([Gonfiatini, 1986](#)).

#### 4.2. Factors affecting the end-member mixing

The weighted-average contribution of freshwater, transition zone and saltwater end-members in the research area were 51.50 %, 36.93 %

and 11.57 %, respectively. Compared with the corresponding 66.05 %, 30.00 % and 3.95 % results using the environmental model with large amounts of measured data from the monitoring station in Minjiang ([Wang et al., 2020](#)), the freshwater contribution in this research was less while that of saltwater was greater. Meanwhile the transition zone's contribution was quite comparable. Over the three months, Spearman analysis revealed the similarity for the contributions of the three end-members when comparing Wang et al.'s results and ours. In fact there was 100 % agreement for the three months.

The highest  $f_s$  occurred in August. In that month, there were important changes in isotopes between flood tide and ebb tide in saltwater zone and salinity was the highest during August. It confirmed that saltwater was dominant in this month. In November, the average of  $\delta D$  and  $\delta^{18}O$  was at a minimum while the d-excess varied in three zones, which suggested that freshwater might have dominated ([Gilfillan, 2002](#)). The higher slope and lower intercept of the  $\delta^{18}O$ -salinity relationship compared to August

and next April during flood tide, which also suggested the influence of freshwater in November (Singh et al., 2010; Kumar and Ramesh, 2017). The  $f_F$  was similar to  $f_T$  in April, while the proximity of  $\delta D$ ,  $\delta^{18}O$  and d-excess for freshwater and transition zone were monitored. All the results showed that the contribution was closely linked to the isotope compositions.

For the freshwater end-member, there were key differences in monthly rainfall and upstream discharge of Shuikou Dam (Fig. 5). In August, a large fluctuation in the daily discharge occurred in the first five days and then it became gentler. The discharge curve in November was the gentlest but in the following April there was a wide variation of discharge with the highest upstream discharge. Referring to the saltwater end-member, the variation in discharge was similar to the upstream discharge. According to the comparison of hydraulic conditions and contributions changes, stable water flow conditions benefited the model's traceability.

In August and November intense evaporation and enrichment occurred, yet the highest  $f_S$  in August and the lowest  $f_S$  in November were calculated, which might have been caused by the high rainfall in August and extreme low rainfall in November, respectively. Meanwhile, the river line in April did indicate precipitation was the main source, and the corresponding medium rainfall led to the  $f_F$  being similar to  $f_T$  in this month. Hence, the model result was related to the meteorological conditions, which strongly suggested the meteorological conditions could shape the modeling outcomes mainly according to the combined influence on the isotopic composition.

## 5. Conclusions

Our field investigations demonstrated that salt intrusion can have a profound impact on isotopes in tidal river scenarios. The average  $\delta D$  and  $\delta^{18}O$  values during the ebb and flood tides in the research area showed distinct intra-annual changes triggered by enriched isotopic in saline water and varying degrees of evaporation in different seasons. The isotopic compositions in August were completely influenced by the oceanic moisture source and local evaporation. Meanwhile in November they were dominated by the freshwater and evaporation and in April were mainly determined by the local moisture source. From upstream to downstream, the isotope values enriched because of the gradually enhanced evaporation. The correlation between isotope index and hydrometeorological indices in the saltwater zone was obviously stronger than that in other zones.

There was no relationship in the freshwater zone and only the d-excess was correlated in transition zone. In the saltwater zone the  $\delta D$  was significantly positively related with temperature and rainfall in the ebb tide and related with humidity, upstream discharge and wind speed in the flood tide, respectively. The humidity, upstream discharge and wind speed were significantly related to  $\delta^{18}O$  and d-excess. The contributions of freshwater end-member, transition zone end-member and saltwater end-member varied according to specific conditions. From August to November to the following April, the  $f_F$  increased from 46.61 % to 60.43 % and then fell to 47.45 %. In the meantime  $f_T$  rose from 32.83 % to 33.66 % then to 44.31 %. However,  $f_S$  reduced from 20.56 % to 5.91 % and then to 8.24 %. The spatiotemporal changes are well explained by the isotopes and meteorological indices. It can be stated here that the annual average contribution does match the results of regional pollution investigations.

## CRedit authorship contribution statement

**Author 1:** Rongrong Xie: Collected the data, Contribution analysis tools, Supervision, Writing- Reviewing and Editing, Revision.

**Author 2:** Ling Zhen: Data curation, performed the analysis, Writing-Original draft preparation, Revision.

**Author 3:** Xianzhong Wu: Collected the data, Supervision.

**Author 4:** Jiabing Li: Collected the data, Supervision, Validation.

## Data availability

Data will be made available on request.

## Declaration of competing interest

The authors declare the following financial interests/personal relationships which may be considered as potential competing interests:

Jiabing Li reports financial support was provided by Fujian Normal University. Rongrong Xie reports financial support was provided by National Natural Science Foundation of China. Jiabing Li reports a relationship with Fujian Normal University that includes: employment. Rongrong Xie reports a relationship with National Natural Science Foundation of China that includes: funding grants.

## Acknowledgments

This work was partially supported by the National Natural Science Foundation of China (42007343) and the Natural Science Foundation of Fujian (2021J01195). The authors extend appreciation to the co-workers who contributed to the field surveys, with especial thanks to Prof. Zuliang Chen. We are also grateful to the journal staff members for their valuable comments on this paper.

## Appendix A. Supplementary data

Supplementary data to this article can be found online at <https://doi.org/10.1016/j.scitotenv.2023.161438>.

## References

- Araguás-Araguás, L., Froehlich, K., 1998. Stable isotope composition of precipitation over southeast Asia. *J. Geophys. Res.* 103, 28721–28742.
- Barlow, P.M., Reichard, E.G., 2010. Saltwater intrusion in coastal regions of North America. *Hydrogeol. J.* 18, 247–260.
- Bauch, D., Schlosser, P., Fairbanks, R.G., 1995. Freshwater balance and the sources of deep and bottom waters in the Arctic Ocean inferred from the distribution of  $H_2^{18}O$ . *Prog. Oceanogr.* 35, 53–80.
- Benetti, M., Reverdin, G., Pierre, C., Merlivat, L., Risi, C., Steen-Larsen, H.C., Vimeux, F., 2014. Deuterium excess in marine water vapor: dependency on relative humidity and surface wind speed during evaporation. *J. Geophys. Res. Atmos.* 119, 584–593.
- Bershaw, J., Penny, S.M., Garzione, C.N., 2012. Stable isotopes of modern water across the Himalaya and eastern Tibetan Plateau: implications for estimates of paleoelevation and paleoclimate. *J. Geophys. Res.* 117, 1–18.
- Bigg, G.R., Rohling, E.J., 2000. An oxygen isotope data set for marine waters. *J. Geophys. Res.* 105, 8527–8535.
- Bryan, E., Meredith, K.T., Baker, A., Andersen, M.S., Treble, P.C., 2019. How water isotopes ( $^{18}O$ ,  $^{2}H$ ,  $^{3}H$ ) within an island freshwater lens respond to changes in rainfall. *Water Res.* 170, 115301.
- Celle-jeanton, H., Travi, Y., Blavoux, B., 2001. Isotopic typology of the precipitation in the Western Mediterranean region at three different time scales. *Geophys. Res. Lett.* 28, 1215–1218.
- Chen, F.J., Huang, C., Lao, Q.B., Zhang, S.W., Chen, C.Q., Zhou, X., Lu, X., Zhu, Q.M., 2021. Typhoon control of precipitation dual isotopes in southern China and its palaeoenvironmental implications. *J. Geophys. Res. Atmos.* 126, e2020JD034336.
- Clark, I.D., Fritz, P., 1997. *Environmental Isotopes in Hydrogeology*. Lewis Publishers, Boca Raton, United States.
- Craig, H., 1961. Isotopic variations in meteoric waters. *Science* 133, 1702–1703.
- Currell, M.J., Dahlhaus, P., Li, H., 2015. Stable isotopes as indicators of water and salinity sources in a southeast Australian coastal wetland: identifying relict marine water, and implications for future change. *Hydrogeol. J.* 23, 235–248.
- Dansgaard, W., 1964. Stable isotopes in precipitation. *Tellus* 16, 436–468.
- Deng, K., Yang, S.Y., Lian, E., Li, C., Yang, C.F., Wei, H.L., 2016. Three Gorges Dam alters the Changjiang (Yangtze) river water cycle in the dry seasons: evidence from H-O isotopes. *Sci. Total Environ.* 562, 89–97.
- Dubinina, E.O., Kossovaa, S.A., Miroshnikov, A.Y., Fyazullina, R.V., 2017. Isotope parameters ( $\delta D$ ,  $\delta^{18}O$ ) and sources of freshwater input to Kara Sea. *Okeanologiya* 57, 38–48.
- Epstein, S., Mayeda, T., 1953. Variation of  $O^{18}$  content of waters from natural sources. *Geochim. Cosmochim. Acta* 4, 213–224.
- Fry, B., 2002. Conservative mixing of stable isotopes across estuarine salinity gradients: a conceptual framework for monitoring watershed influences on downstream fisheries production. *Estuaries* 25, 264–271.
- Gammons, C.H., Poulson, S.R., Pellicori, D.A., Reed, P.J., Roesler, A.J., Petrescu, E.M., 2006. The hydrogen and oxygen isotopic composition of precipitation, evaporated mine water, and river water in Montana, USA. *J. Hydrol.* 328, 319–330.
- Gao, Q., Li, Y., Qi, Z., Yue, Y., Min, M., Peng, S., Shi, Z., Gao, Y., 2018. Diverse and abundant antibiotic resistance genes from mariculture sites of China's coastline. *Sci. Total Environ.* 630, 117–125.
- Gat, J.R., 1996. Oxygen and hydrogen isotopes in the hydrologic cycle. *Annu. Rev. Earth Planet. Sci.* 24, 225–262.



- Gibson, J.J., Aggarwal, P., Hogan, J., Kendall, C., Martinelli, L.A., Stichler, W., Rank, D., Goni, I., Choudhry, M., Gat, J., Bhattacharya, S., Sugimoto, A., Fekete, B., Pietroniro, A., Maurer, T., Panarello, H., Stone, D., Seyler, P., Maurice-Bourgoin, L., Herczeg, A., 2002. Isotope studies in large river basins: a new global research focus. *Eos Trans. Am. Geophys. Union* 83, 613–620.
- Gibson, J.J., Edwards, T.W.D., Birks, S.J., Amour, N.A.S., Buhay, W.M., McEachern, P., Wolfe, B.B., Peters, D.L., 2005. Progress in isotope tracer hydrology in Canada. *Hydrol. Process.* 19, 303–327.
- Gilfillan, E.S., 2002. The isotopic composition of sea water. *J. Am. Chem. Soc.* 56, 406–408.
- Gonfiatini, R., 1986. Environmental isotopes in Lake studies. *Handbook of Environmental Isotope Geochemistry; The Terrestrial Environment*. Elsevier B.V., pp. 113–168.
- Gong, W.P., Shen, J., 2011. The response of salt intrusion to changes in river discharge and tidal mixing during the dry season in the Modaomen Estuary, China. *Cont. Shelf Res.* 31, 769–788.
- Grassa, F., Favara, R., Valenza, M., 2006. Moisture source in the Hyblean Mountains region (south-eastern Sicily, Italy): evidence from stable isotopes signature. *Appl. Geochem.* 21, 2082–2095.
- Gross, E., Andrews, S., Bergamaschi, B., Downing, B., Holleman, R., Burdick, S., Durand, J., 2019. The use of stable isotope-based water age to evaluate a hydrodynamic model. *Water* 11, 2207.
- Guo, L., Xiu, P., Chai, F., Xue, H.J., Wang, D.X., Sun, J., 2017. Enhanced chlorophyll concentrations induced by Kuroshio intrusion fronts in the Northern South China Sea. *Geophys. Res. Lett.* 44, 11565–11572.
- Guo, X.J., Tang, Y.C., Xu, Y., Zhang, S.S., Ma, J., Xiao, S.B., Ji, D.B., Yang, Z.J., Liu, D.F., 2020. Using stable nitrogen and oxygen isotopes to identify nitrate sources in the Lancang River, upper Mekong. *J. Environ. Manag.* 274, 111197.
- Harvey, F.E., Welker, J.M., 2000. Stable isotopic composition of precipitation in the semi-arid north-central portion of the US Great Plains. *J. Hydrol.* 238, 90–109.
- Heiss, J.W., Post, V.E.A., Laattoe, T., Russoniello, C.J., Michael, H.A., 2017. Physical controls on biogeochemical processes in intertidal zones of beach aquifers. *Water Resour. Res.* 53, 9225–9244.
- Hu, M.P., Liu, Y.M., Zhang, Y.F., Dahlgren, R.A., Chen, D.J., 2018. Coupling stable isotopes and water chemistry to assess the role of hydrological and biogeochemical processes on riverine nitrogen sources. *Water Res.* 150, 418–430.
- Hu, X.S., Wu, C.Z., Hong, W., Qiu, R.Z., Li, J., Hong, T., 2014. Forest cover change and its drivers in the upstream area of the Minjiang River, China. *Ecol. Indic.* 46, 121–128.
- Hu, Y., Liu, G.D., Meng, Y.C., Zhang, W.J., Xie, C.C., 2019. Analysis of stable hydrogen and oxygen isotope characteristics and vapor sources of event-based precipitation in Chengdu. *Environ. Sci.* 40, 1179–1187 (in Chinese).
- Huang, W.Y., He, X.S., Yang, Z.F., Qiu, T.P., Wright, J.S., Wang, B., Lin, D.Y., 2018. Moisture sources for wintertime extreme precipitation events over South China during 1979–2013. *J. Geophys. Res. Atmos.* 123, 6690–6712.
- Ji, X.L., Xie, R.T., Hao, Y., Lu, J., 2017. Quantitative identification of nitrate pollution sources and uncertainty analysis based on dual isotope approach in an agricultural watershed. *Environ. Pollut.* 229, 586–594.
- Jung, H.J., Koh, D.C., Kim, Y.S., Jeon, S.W., Lee, J., 2020. Stable isotopes of water and nitrate for the identification of groundwater flowpaths: a review. *Water* 12, 138.
- Ke, S., Chen, J., Zheng, X., 2021. Influence of the subsurface physical barrier on nitrate contamination and seawater intrusion in an unconfined aquifer. *Environ. Pollut.* 284, 117528.
- Kopec, B.G., Feng, X., Posmentier, E.S., Sonder, L.J., 2018. Seasonal deuterium excess variations of precipitation at Summit, Greenland, and their climatological significance. *J. Geophys. Res. Atmos.* 124, 72–91.
- Kumar, K.P., Ramesh, R., 2017. Revisiting reconstructed Indian monsoon rainfall variations during the last ~25 ka from planktonic foraminiferal  $\delta^{18}\text{O}$  from the Eastern Arabian Sea. *Quat. Int.* 443, 29–38.
- Kumar, K.P., Singh, A., Ramesh, R., 2018. Controls on  $\delta^{18}\text{O}$ ,  $\delta\text{D}$  and  $\delta^{18}\text{O}$ -salinity relationship in the northern Indian Ocean. *Mar. Chem.* 207, 55–62.
- Lao, Q., Wu, J., Chen, F., Zhou, X., Li, Z., Chen, C., Zhu, Q., Deng, Z., Li, J., 2022a. Increasing intrusion of high salinity water alters the mariculture activities in Zhanjiang Bay during the past two decades identified by dual water isotopes. *J. Environ. Manag.* 320, 115815.
- Lao, Q., Zhang, S., Li, Z., Chen, F., Zhou, X., Jin, G., Huang, P., Deng, Z., Chen, C., Zhu, Q., Lu, X., 2022b. Quantification of the seasonal intrusion of water masses and their impact on nutrients in the Beibu Gulf using dual water isotopes. *J. Geophys. Res. Oceans* 127 (7), e2021JC018065.
- Li, G., Zhang, X.P., Xu, Y.P., Song, S., Wang, Y.F., Ji, X.M., Xiang, J., Yang, J., 2016. Characteristics of stable isotopes in precipitation and their moisture sources in Mengzi Region, Southern Yunnan. *Environ. Sci.* 37, 1313–1320 (in Chinese).
- Lian, E.G., Yang, S.Y., Wu, H., Yang, C.F., Li, C., Liu, J.T., 2016. Kuroshio subsurface water feeds the wintertime Taiwan Warm Current on the inner East China Sea shelf. *J. Geophys. Res. Oceans* 121, 4790–4803.
- Liss, P.S., 1976. Conservative and non-conservative behavior of dissolved constituents during estuarine mixing. *Estuar. Chem. Academic Press, London*, pp. 93–130.
- Liu, B.J., Liao, Y.Y., Yan, S.L., Yan, H.H., 2017. Dynamic characteristics of saltwater intrusion in the Pearl River Estuary, China. *Nat. Hazards* 89, 1097–1117.
- Liu, H.T., Guo, Z.R., Gao, A.G., Yuan, X.J., Zhang, B., 2016. O-18 and Ra-226 in the Minjiang River estuary, China and their hydrological implications. *Estuar. Coast. Shelf Sci.* 173, 93–101.
- Loder, T.C., Reichard, R.P., 1981. The dynamics of conservative mixing in estuaries. *Estuaries* 4, 64–69.
- Masson-Delmotte, V., Hou, S., Ekaykin, A., Jouzel, J., Aristarain, A., Bernardo, R., Bromwich, D., Cattani, O., Delmotte, M., Falourd, S., 2008. A review of Antarctic surface snow isotopic composition: observations, atmospheric circulation, and isotopic modeling. *J. Clim.* 21, 3359–3387.
- Matsuo, S., Friedman, I., 1967. Deuterium content in fractionally collected rainwater. *J. Geophys. Res.* 72, 6374–6376.
- May, L.B., Richard, A.J., Michael, A.M., 2010. Hydrodynamic behavior of the cape fear river and estuarine system: a synthesis and observational investigation of discharge-salinity intrusion relationships. *Estuar. Coast. Shelf Sci.* 88, 407–418.
- Méès, L., Grosjean, N., Marié, J.L., 2020. Statistical Lagrangian evaporation rate of droplets released in a homogeneous quasi-isotropic turbulence. *Phys. Rev. Fluids* 5, 113602.
- Merlivat, L., Jouzel, J., 1979. Global climatic interpretation of the deuterium-oxygen 18 relationship for precipitation. *J. Geophys. Res.* 84, 5029–5033.
- Natali, S., Banerjee, I., Doveri, M., Gnanecchini, R., Selmo, E., Zanchetta, G., 2021. Meteorological and geographical control on stable isotopic signature of precipitation in a western Mediterranean area (Tuscany, Italy): disentangling a complex signal. *J. Hydrol.* 603, 126944.
- Neubauer, S.C., 2013. Ecosystem responses of a tidal freshwater marsh experiencing saltwater intrusion and altered hydrology. *Estuar. Coasts* 36, 491–507.
- Niu, C., Zhai, T.L., Zhang, Q.Q., Wang, H.W., Xiao, L.L., 2021. Research advances in the analysis of nitrate pollution sources in a freshwater environment using  $\delta^{15}\text{N}$ -NO<sub>3</sub> – and  $\delta^{18}\text{O}$ -NO<sub>3</sub> –. *Environ. Res. Public Health* 18, 11805.
- Nuttle, W.K., Fourqurean, J.W., Cosby, B.J., Ziemann, J.C., Robblee, M.B., 2000. Influence of net freshwater supply on salinity in Florida Bay. *Water Resour. Res.* 36, 1805–1822.
- Oza, H., Padhya, V., Ganguly, A., Deshpande, R.D., 2022. Investigating hydrometeorology of the Western Himalayas: insights from stable isotopes of water and meteorological parameters. *Atmos. Res.* 268, 105997.
- Parnell, A.C., Inger, R., Bearhop, S., Jackson, A.L., 2010. Source partitioning using stable isotopes: coping with too much variation. *Plos One* 5, e9672.
- Paulsson, O., Wunderlund, A., 2020. Pit lake oxygen and hydrogen isotopic composition in subarctic Sweden: a comparison to the local meteoric water line. *Appl. Geochem.* 118, 104611.
- Peng, H.D., Mayer, B., Norman, A.L., Krouse, H.R., 2005. Modelling of hydrogen and oxygen isotope compositions for local precipitation. *Tellus Ser. B Chem. Phys. Meteorol.* 57, 273–282.
- Phillips, D.L., 2001. Mixing models in analyses of diet using multiple stable isotopes a critique. *Oecologia* 127, 166–170.
- Phillips, D.L., Gregg, J.W., 2001. Uncertainty in source partitioning using stable isotopes. *Oecologia* 127, 171–179.
- Price, R.M., Skrzypek, G., Grierson, P.F., Swart, P.K., Fourqurean, J.W., 2012. The use of stable isotopes of oxygen and hydrogen to identify water sources in two hypersaline estuaries with different hydrologic regimes. *Mar. Freshw. Res.* 63, 952–966.
- Puscas, R.H., 2019. Correlation of the stable hydrogen and oxygen isotopes with the atmospheric humidity from Cluj-Napoca, Romania. *Anal. Lett.* 54, 1–11.
- Reyes-Macaya, D., Hoogakker, B., Martínez-Méndez, G., Llanillo, P.J., Grasse, P., Mohtadi, M., Mix, A., Leng, M.J., Struck, U., McCorkle, D.C., Troncoso, M., Gayo, E.M., Lange, C.B., Farias, L., Carhuapoma, W., Graco, M., Ottone, M.C., Holz, R.D.P., Fernandez, C., Narvaez, D., Vargas, C.A., Gracia-Araya, F., Hebbeln, D., 2022. Isotopic characterization of water masses in the Southeast Pacific region: paleoceanographic implications. *J. Geophys. Res. Oceans* 127, e2021JC017525.
- Schiavo, M.A., Hauser, S., Povinec, P.P., 2009. Stable isotopes of water as a tool to study groundwater-seawater interactions in coastal south-eastern Sicily. *J. Hydrol.* 364, 40–49.
- Sengupta, S., Parekh, A., Chakraborty, S., Kumar, K.R., Bose, T., 2013. Vertical variation of oxygen isotope in Bay of Bengal and its relationships with water masses. *J. Geophys. Res. Oceans* 118, 6411–6424.
- Simmons, A.J., Willett, K.M., Jones, P.D., Thorne, P.W., Dee, D.P., 2010. Low-frequency variations in surface atmospheric humidity, temperature, and precipitation: inferences from reanalyses and monthly gridded observational data sets. *J. Geophys. Res.* 115, D1.
- Singh, A., Jani, R.A., Ramesh, R., 2010. Spatiotemporal variations of the  $\delta^{18}\text{O}$ -salinity relation in the northern Indian Ocean. *Deep-Sea Res. I Oceanogr. Res. Pap.* 57, 1422–1431.
- Singh, A., Mohiuddin, A., Ramesh, R., Raghav, S., 2014. Estimating the loss of Himalayan glaciers under global warming using the  $\delta^{18}\text{O}$ -salinity relation in the Bay of Bengal. *Environ. Sci. Technol. Lett.* 1, 249–253.
- Spiker, E.C., 1980. The behavior of  $^{14}\text{C}$  and  $^{13}\text{C}$  in estuarine water: effects of in situ CO<sub>2</sub> production and atmospheric exchange. *Radiocarbon* 22, 647–654.
- Stalker, J.C., Price, R.M., Swart, P.K., 2009. Determining spatial and temporal inputs of freshwater, including submarine groundwater discharge, to a subtropical estuary using geochemical tracers, Biscayne Bay, South Florida. *Estuar. Coasts* 32, 694–708.
- Tian, L., Liu, Z.F., Gong, T.L., Yin, C.L., Yu, W.S., Yao, T.D., 2008. Isotopic variation in the lake water balance at the Yamdruk-tso basin, southern Tibetan Plateau. *Hydrol. Process.* 22, 3386–3392.
- Tian, L.D., Yao, T.D., Sun, W.Z., Stievenard, M., Jouzel, J., 2001. Relationship between  $\delta\text{D}$  and  $\delta^{18}\text{O}$  in precipitation on north and south of the Tibetan Plateau and moisture recycling. *Sci. China Earth Sci.* 44, 789–796.
- UNESCO, 1985. The international system of units (SI) in oceanography. *UNESCO Tech. Pap. Mar. Sci.* 45. IAPSO Publication Scientifique, p. 42.
- Wang, J., Zhu, T.Y., Pang, Y., Li, S., 2020. Study on sources of inorganic nitrogen pollution in Minjiang Estuary coastal waters. *Si Chuan Environ.* 39, 15–23 (in Chinese).
- Werner, A.D., Bakker, M., Post, V.E.A., Vandenbohede, A., Lu, C.H., Ataie-Ashtiani, B., Simmons, C.T., Barry, D.A., 2013. Seawater intrusion processes, investigation and management: recent advances and future challenges. *Adv. Water Resour.* 51, 3–26.
- Wu, H., Zhang, X., Xiao, Y.L., Li, G., Huang, Y.M., 2015. Seasonal variations of deuterium and oxygen-18 isotopes and their response to moisture source for precipitation events in the subtropical monsoon region. *Hydrol. Process.* 29, 90–102.
- Wu, H.W., Song, F., Li, J., Zhou, Y.Q., Zhang, J.M., Fu, C.S., 2022. Surface water isoscapes ( $\delta^{18}\text{O}$  and  $\delta^2\text{H}$ ) reveal dual effects of damming and drought on the Yangtze River water cycles. *J. Hydrol.* 610, 127847.
- Wu, J.H., Lao, Q.B., Chen, F.J., Chao, H., Zhang, S.W., Wang, C., Zhou, F.X., Chen, C.Q., Zhou, X., Lu, X., 2021. Water mass processes between the South China Sea and the Western Pacific through the Luzon Strait: insights from hydrogen and oxygen isotopes. *J. Geophys. Res. Oceans* 126, e2021JC017484.



- Wu, S.Y., Tan, D.Y., Lewis, S., Tian, L.D., Ma, Y.M., Xu, B.Q., Qu, D.M., 2014. Stable oxygen isotope differences between the areas to the north and south of Qinling Mountains in China reveal different moisture sources. *Int. J. Climatol.* 34, 1760–1772.
- Xia, Z.Y., Welker, J.M., Winnick, M.J., 2022. The seasonality of deuterium excess in non-polar precipitation. *Glob. Biogeochem. Cycles* 36, e2021GB007245.
- Xie, R.R., Pang, Y., Luo, B.L., Li, J.B., Wu, C.S., Zheng, Y.Y., Sun, Q.Y., Zhang, P., Wang, F.F., 2017. Spatiotemporal variability in salinity and hydraulic relationship with salt intrusion in the tidal reaches of the Minjiang River, Fujian Province, China. *Environ. Sci. Pollut. Res.* 24, 11847–11855.
- Xie, R.R., Rao, P.Y., Pang, Y., Shi, C.H., Li, J.B., Shen, D.D., 2020. Salt intrusion alters nitrogen cycling in tidal reaches as determined in field and laboratory investigations. *Sci. Total Environ.* 729, 138803.
- Xiong, H., Jia, W.X., Zhu, G.F., Ma, X.G., Xu, X.T., Yuan, R.F., Zhang, Z.Y., Shi, Y., Yang, L., 2021. Influence of below-cloud secondary evaporation on stable isotope composition in precipitation and its relationship with meteorological factors in Shiyang River Basin, Northwest China. *Environ. Earth Sci.* 80, 255.
- Xu, M.N., Zhang, W.J., Zhu, Y.F., Liu, L., Zheng, Z.Z., Wan, X.H., Qian, W., Dai, M.H., Gan, J.P., Hutchins, D.A., Kao, S., 2018. Enhanced ammonia oxidation caused by lateral Kuroshio intrusion in the boundary zone of the northern South China Sea. *Geophys. Res. Lett.* 45, 6585–6593.
- Xu, R.C., Pang, Y., Hu, Z.B., Wang, J.J., Kaisam, J.P., 2020. Study on pollution traceability based on the optimized hydrodynamic model of Tai Lake. *Water Sci. Technol. Water Supply* 20, 3014–3028.
- Xue, D.M., Baets, B.D., Cleemput, O.V., Hennessy, C., Berglund, M., Boeckx, P., 2012. Use of a Bayesian isotope mixing model to estimate proportional contributions of multiple nitrate sources in surface water. *Environ. Pollut.* 161, 43–49.
- Zannoni, D., Steen-Larsen, H.C., Rampazzo, G., Dreossi, G., Stenni, B., Bergamasco, A., 2019. The atmospheric water cycle of a coastal lagoon: an isotope study of the interactions between water vapor, precipitation and surface waters. *J. Hydrol.* 572, 630–644.
- Zhang, B., Guo, Z.R., Gao, A.J., Yuan, X.J., Li, K.P., 2013. An analysis of the interaction between river water, groundwater and seawater in Minjiang River Estuary Region, Fujian Province, based on stable isotopes D and  $^{18}\text{O}$ . *Acta Geosci. Sin.* 34, 213–222 (in Chinese).
- Zhang, P., Pang, Y., Pan, H.C., Shi, C.C., Huang, Y.W., Wang, J.J., 2015. Factors contributing to hypoxia in the Minjiang River Estuary, Southeast China. *Int. J. Environ. Res. Public Health* 12, 9357–9374.
- Zhang, P., Pang, Y., Shi, C.C., Wang, Y.S., Xu, L., Pan, H.C., Xie, R.R., 2016. Analysis and numerical simulation of natural and human-caused low dissolved oxygen in the Minjiang River Estuary. *Water Sci. Technol.* 73, 2475–2485.
- Zhou, F.X., Wu, J.H., Chen, F.J., Chen, C.Q., Zhu, Q.M., Lao, Q.B., Zhou, X., Lu, X., 2022. Using stable isotopes ( $\delta^{18}\text{O}$  and  $\delta\text{D}$ ) to study the dynamics of upwelling and other oceanic processes in northwestern South China Sea. *J. Geophys. Res. Oceans* 127, e2021JC017972.